Supplement of Nat. Hazards Earth Syst. Sci., 21, 2753–2772, 2021
https://doi.org/10.5194/nhess-21-2753-2021-supplement

Natural Hazards and Earth System Sciences
Open Access
EGU

Supplement of

Timely prediction potential of landslide early warning systems with multispectral remote sensing: a conceptual approach tested in the Sattelkar, Austria

Doris Hermle et al.

Correspondence to: Doris Hermle (doris.hermle@tum.de)

Online supplementary material

Figure S1 Overview of UAS flight path with GCP distribution.

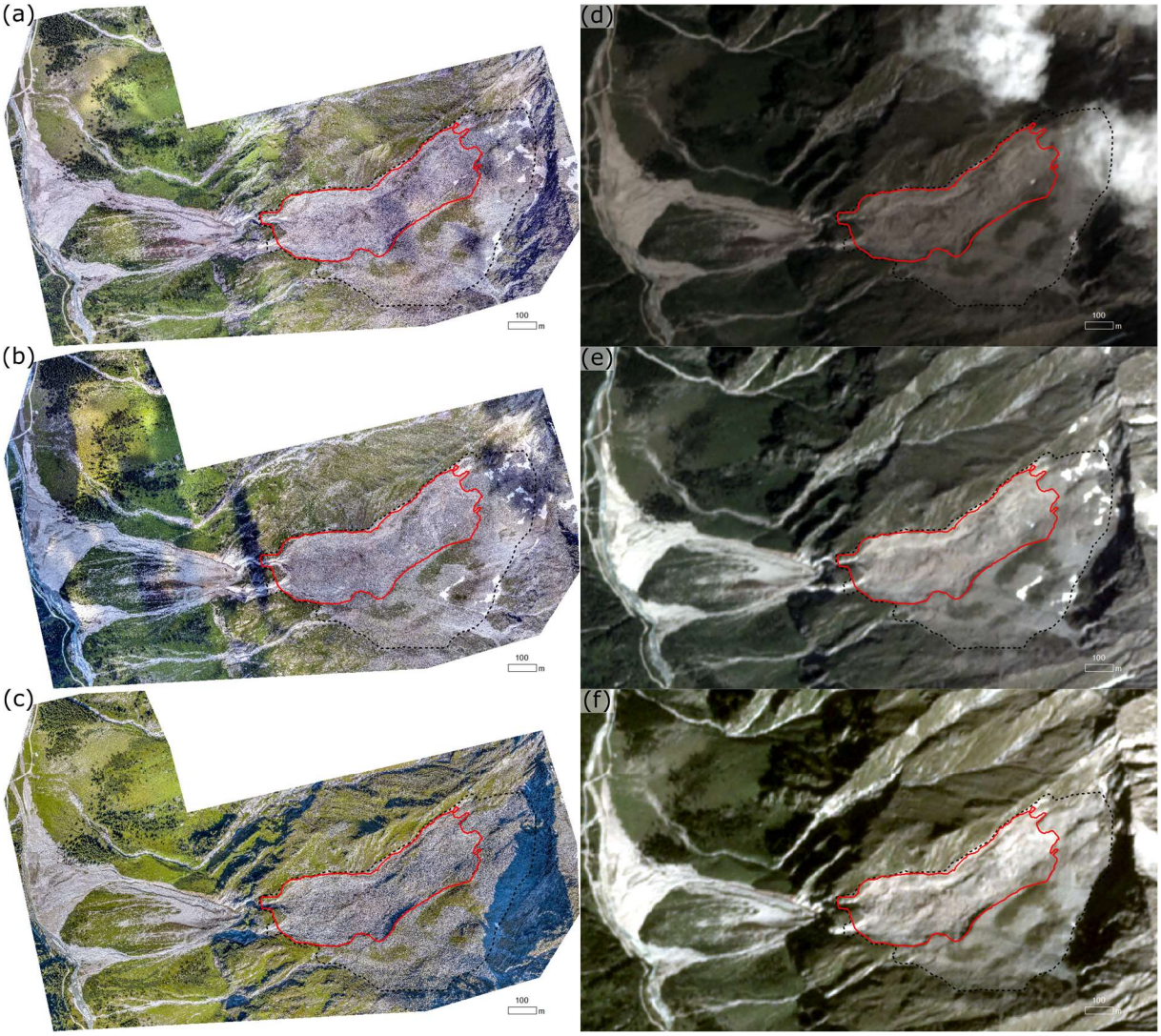

Figure S2 Input data of UAS orthoimages at 0.16 m resolution (a) 13.07.2018, (b) 24.07.2019, (c) 04.09.2019 and PlanetScope satellite images at 3 m resolution (d) 19.07.2018, (e) 24.07.2019, (f) 04.09.2019.

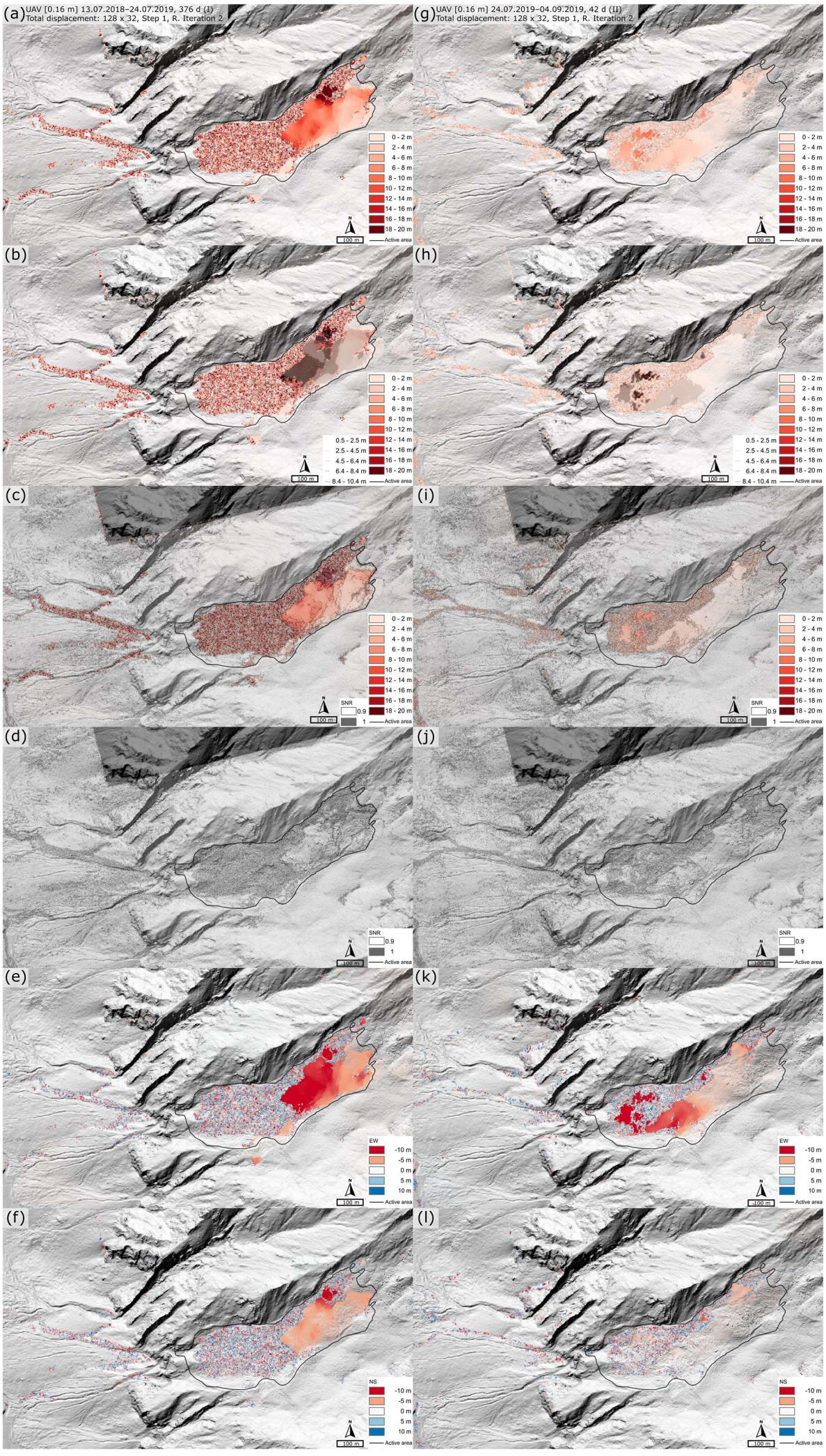
(a)
UAV [0.16 m] 13.07.2018–24.07.2019, 376 d (I)
Total displacement: 128 x 32, Step 1, R. Iteration 2
(g)
UAV [0.16 m] 24.07.2019–04.09.2019, 42 d (II)
Total displacement: 128 x 32, Step 1, R. Iteration 2
(b)
(h)
(c)
(i)
(d)
(j)
(e)
(k)
(f)
(l)
0 - 2 m
2 - 4 m
4 - 6 m
6 - 8 m
8 - 10 m
10 - 12 m
12 - 14 m
14 - 16 m
16 - 18 m
18 - 20 m
0.5 - 2.5 m
2.5 - 4.5 m
4.5 - 6.4 m
6.4 - 8.4 m
8.4 - 10.4 m
SNR
0.9
1
EW
NS
-10 m
-5 m
0 m
5 m
10 m
Active area
100 m

Figure S3 DIC outputs for Interval I (13.07.2018–24.07.2019, 376 d) and II (24.07.2019–04.09.2019, 42 d) of UAS orthophotos at 0.16 m resolution for COSI–Corr parameter settings 128 x 32, step size 1 and 2 robustness iterations. Interval I (a) and II (g) are total displacements; (b) and (h) show total displacement with vectors filtered for a direction between 205° and 280° and a length larger than 0.5 m; (c) and (i) display the total displacement in combination with the result of signal–to–noise calculations (40 % transparency); (d) and (j) are only signal–to–noise calculations (40 % transparency). The last two rows show displacements of East–West orientation for (e) and (k) while North–South are orientations for (f) and (l) prior to total displacement calculations. The solid black line represents the boundary of the active landslide based on field mapping. Background: hillshade of Lidar DEM, 1 m resolution (© SAGIS).

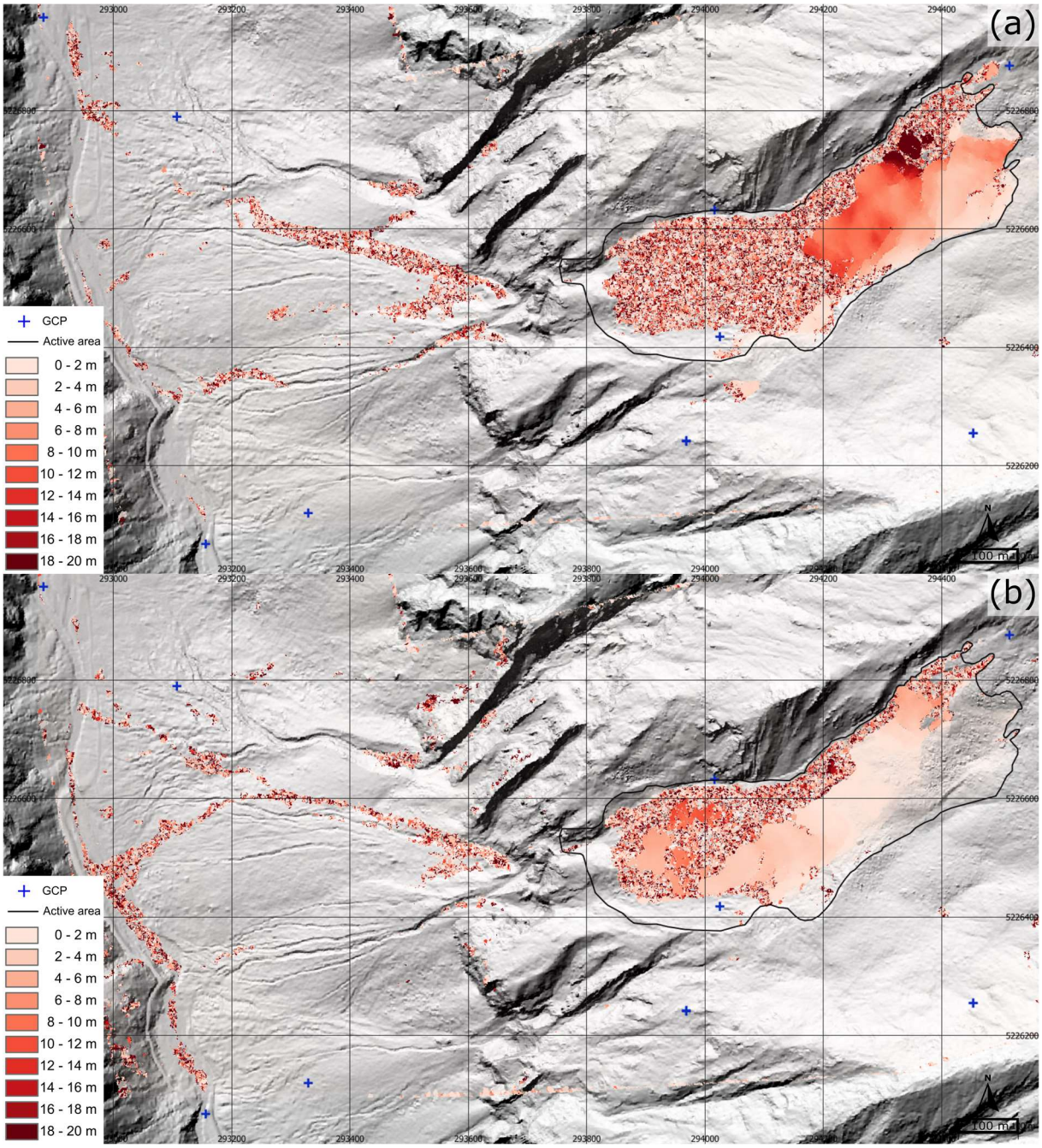

Figure S4 DIC outputs for (a) Interval I (13.07.2018–24.07.2019, 376 d) and (b) II (24.07.2019–04.09.2019, 42 d) of UAS orthophotos at 0.16 m resolution for COSI–Corr parameter settings 128 x 32, step size 1 and 2 robustness iterations. Blue crosses indicate GCP distribution. The solid black line represents the boundary of the active landslide based on field mapping. Background: hillshade of Lidar DEM, 1 m resolution (© SAGIS).

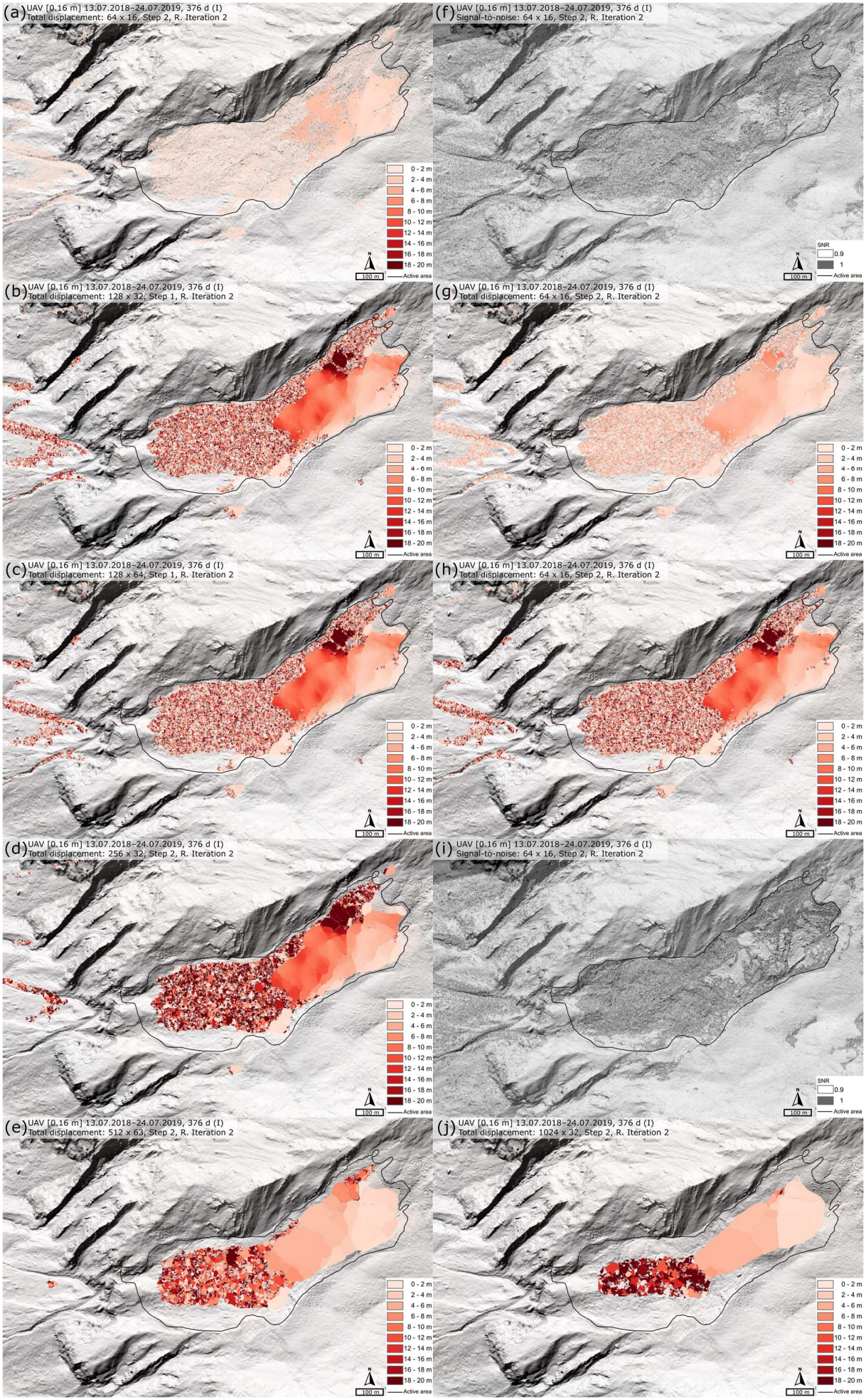

Figure S5 DIC total displacements for Interval I (13.07.2018–24.07.2019, 376 d) at 0.16 m resolution with different parameter setting combinations and signal–to–noise calculations for (f) and (i), both displayed with 40 % transparency. The

solid black line represents the boundary of the active landslide based on field mapping. Background: hillshade of Lidar DEM, 1 m resolution (© SAGIS).

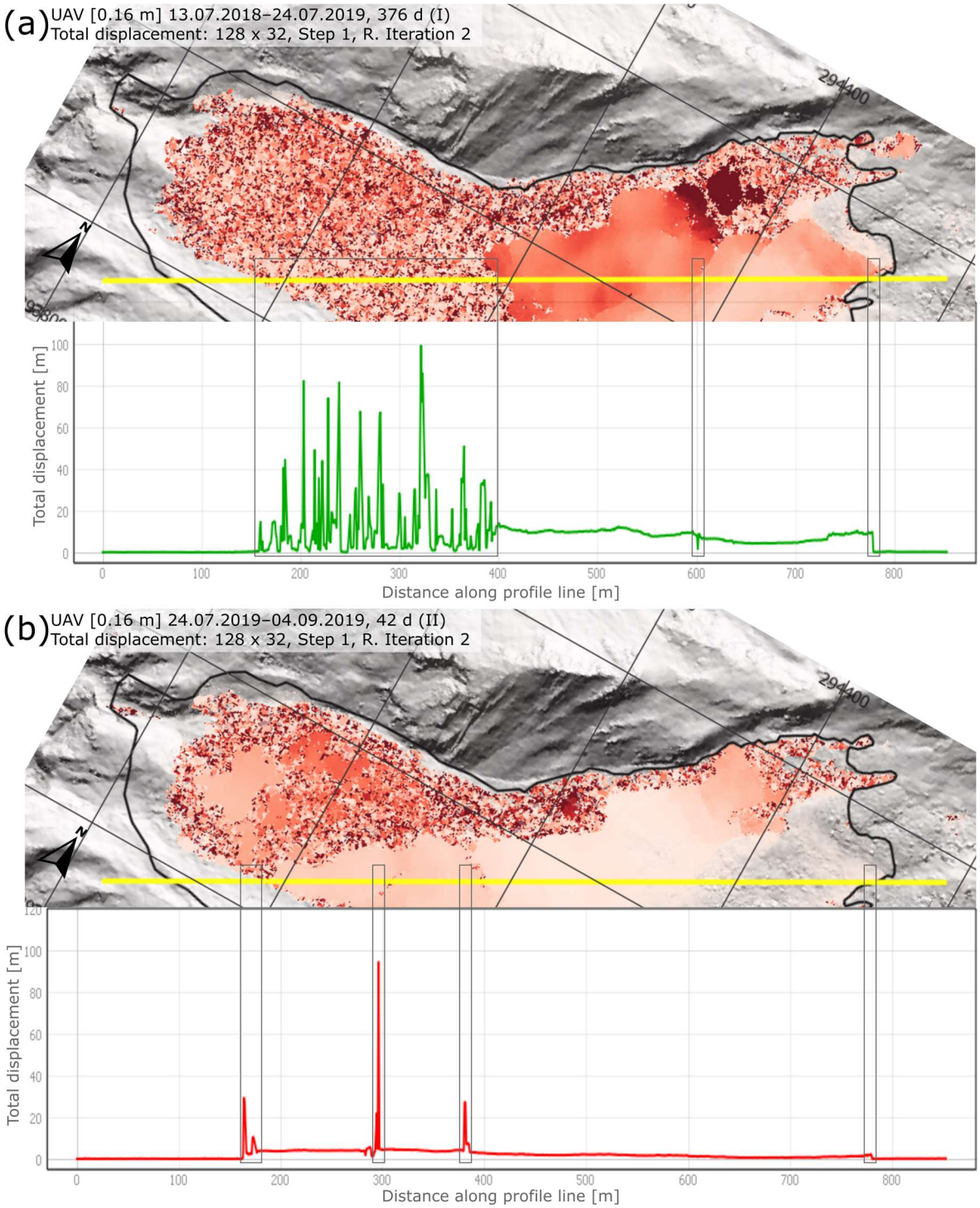

Figure S6 Identical profiles for total displacement for (a) Interval I (13.07.2018–24.07.2019, 376 d) and (b) II (24.07.2019–04.09.2019, 42 d) of UAS orthophotos at 0.16 m resolution for COSI–Corr parameter settings 128 x 32, step size 1 and 2 robustness iterations. Yellow profile line is identical for (a) and (b) with corresponding profiles below. Grey outline bars point to distinct changes in profile and DIC result. The solid black line represents the boundary of the active landslide based on field mapping. Background: hillshade of Lidar DEM, 1 m resolution (© SAGIS).

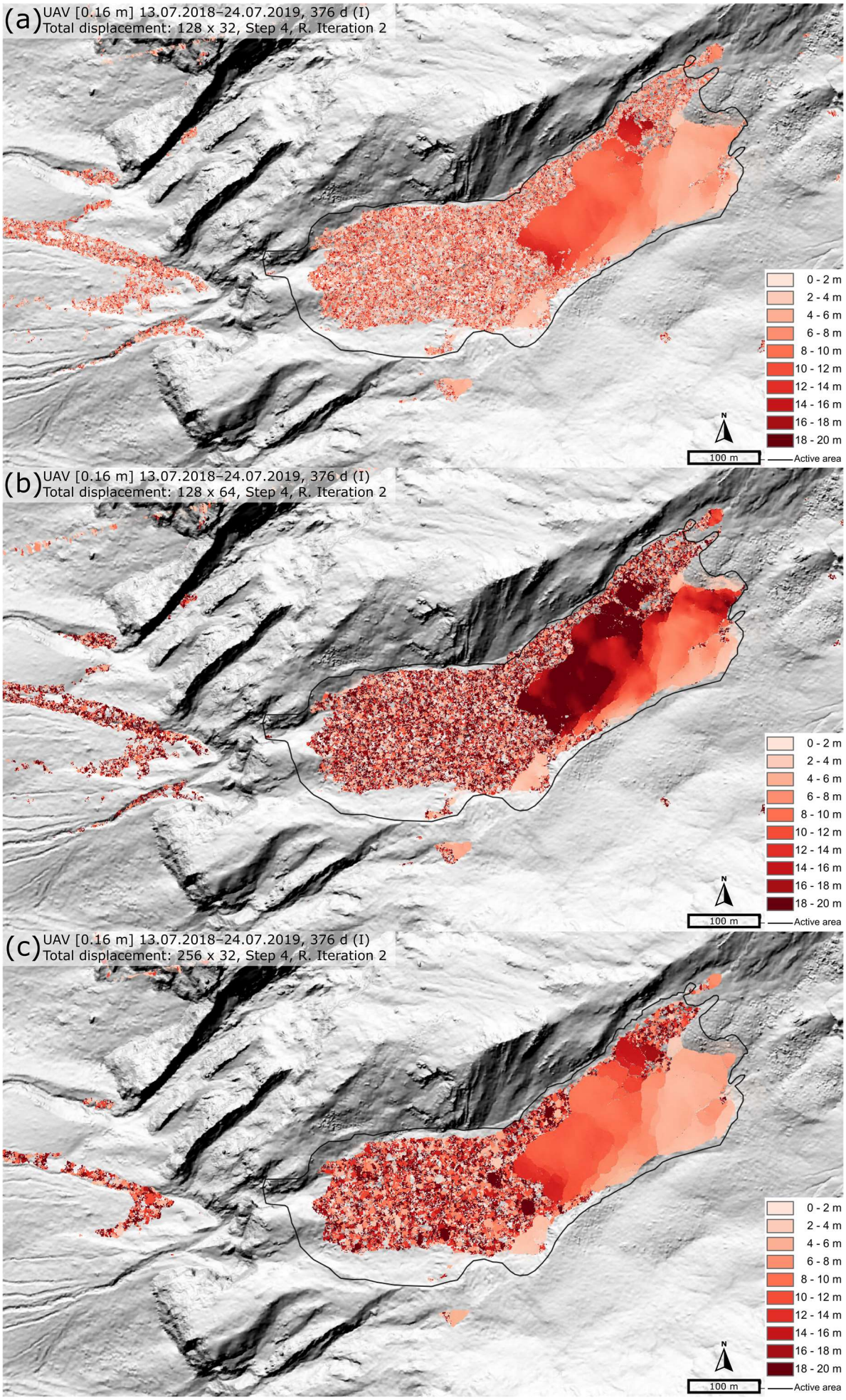

Figure S7 DIC total displacements for Interval I (13.07.2018–24.07.2019, 376 d) at 0.16 m resolution with different window setting combinations for step size 4. The solid black line represents the boundary of the active landslide based on field mapping. Background: hillshade of Lidar DEM, 1 m resolution (© SAGIS).

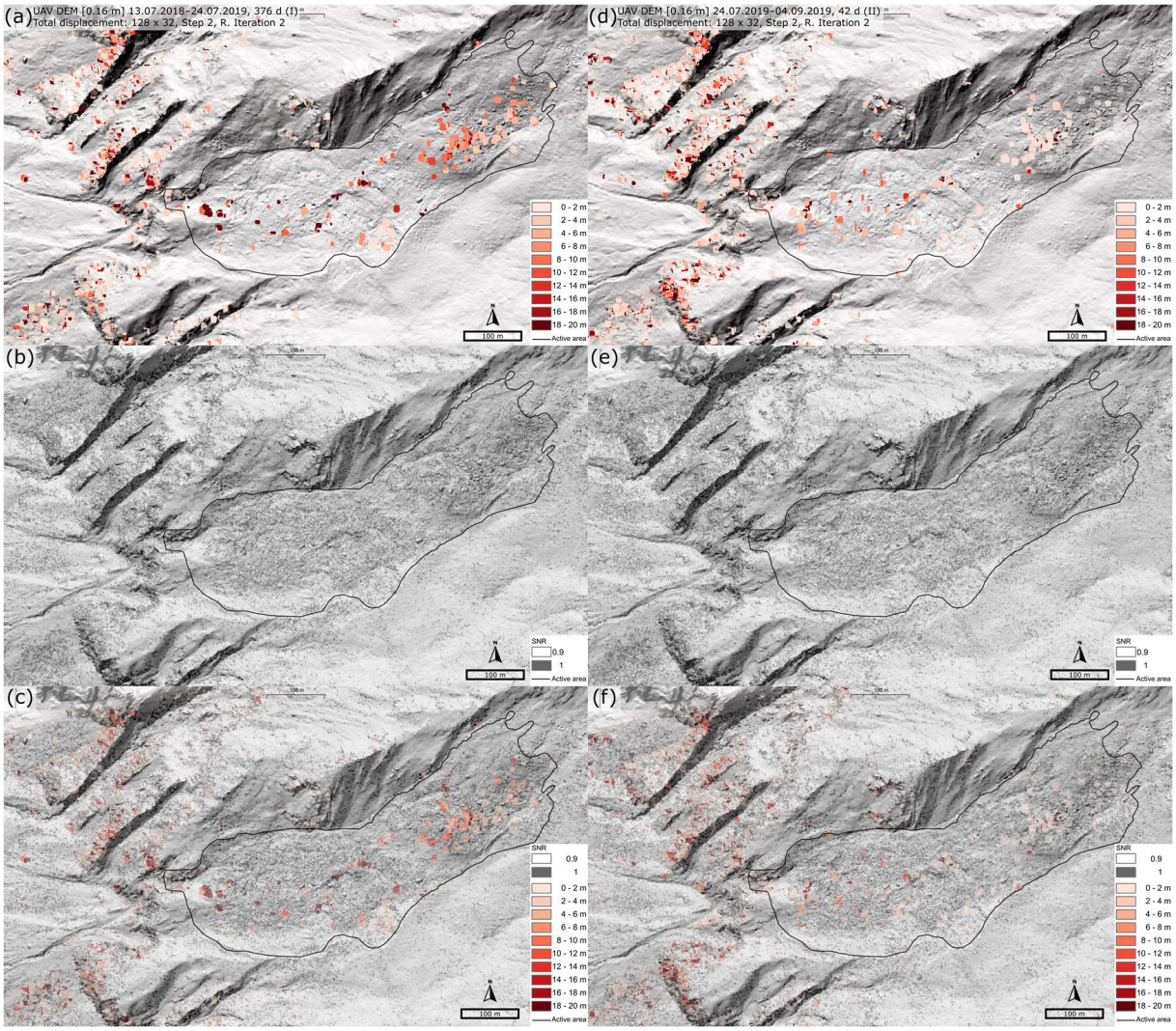

Figure S8 Results of DIC total displacement calculations of UAS DSM at 0.16 m resolution with COSI-Corr for both Intervals I (13.07.2018–24.07.2019, 376 d) and II (24.07.2019–04.09.2019, 42 d). Parameter settings were 128 x 32, step size 2 with 2 robustness iterations. The solid black line represents the boundary of the active landslide based on field mapping. Background: hillshade of Lidar DEM, 1 m resolution (© SAGIS).

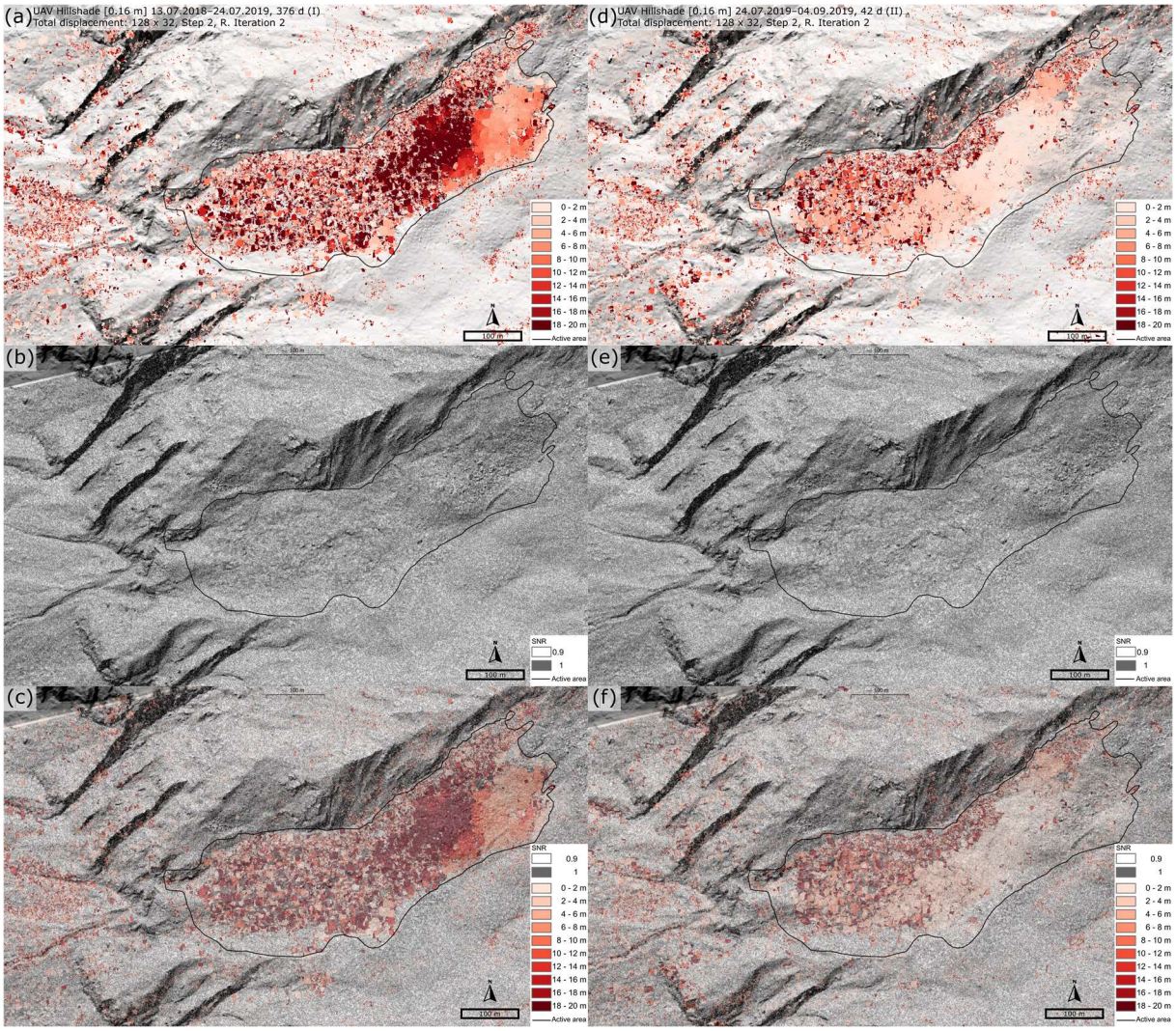

Figure S9 Results of DIC total displacement calculations of UAS hillshades at 0.16 m resolution with COSI-Corr for both Intervals I (13.07.2018–24.07.2019, 376 d) and II (24.07.2019–04.09.2019, 42 d). Parameter settings were 128 x 32, step size 2 with 2 robustness iterations. The solid black line represents the boundary of the active landslide based on field mapping. Background: hillshade of Lidar DEM, 1 m resolution (© SAGIS).

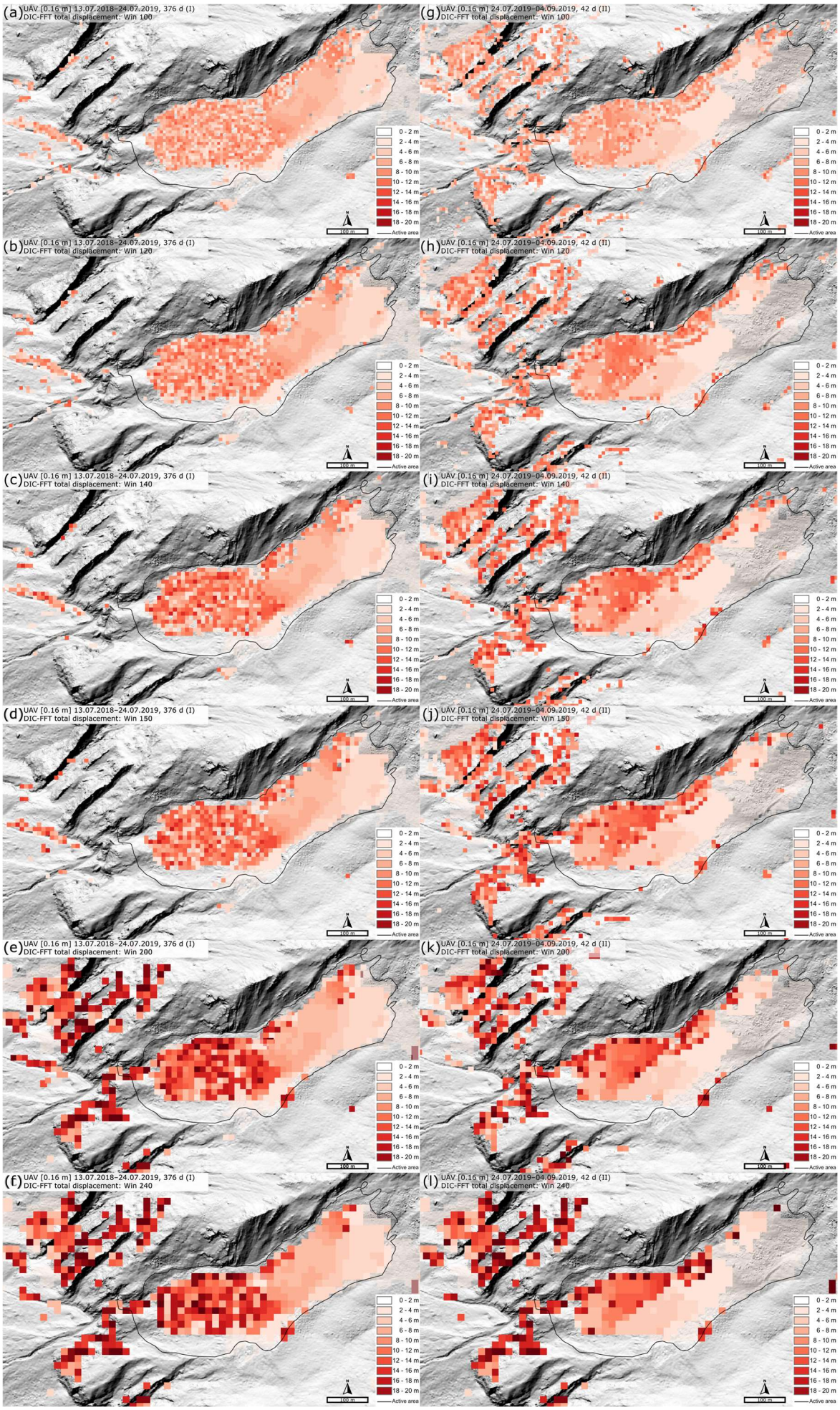

Figure S10 Total displacement results of DIC-FFT tool of UAS orthoimages at 0.16 m resolution for interval I and II with different window size parameters. The solid black line represents the boundary of the active landslide based on field mapping. Background: hillshade of Lidar DEM, 1 m resolution (© SAGIS).

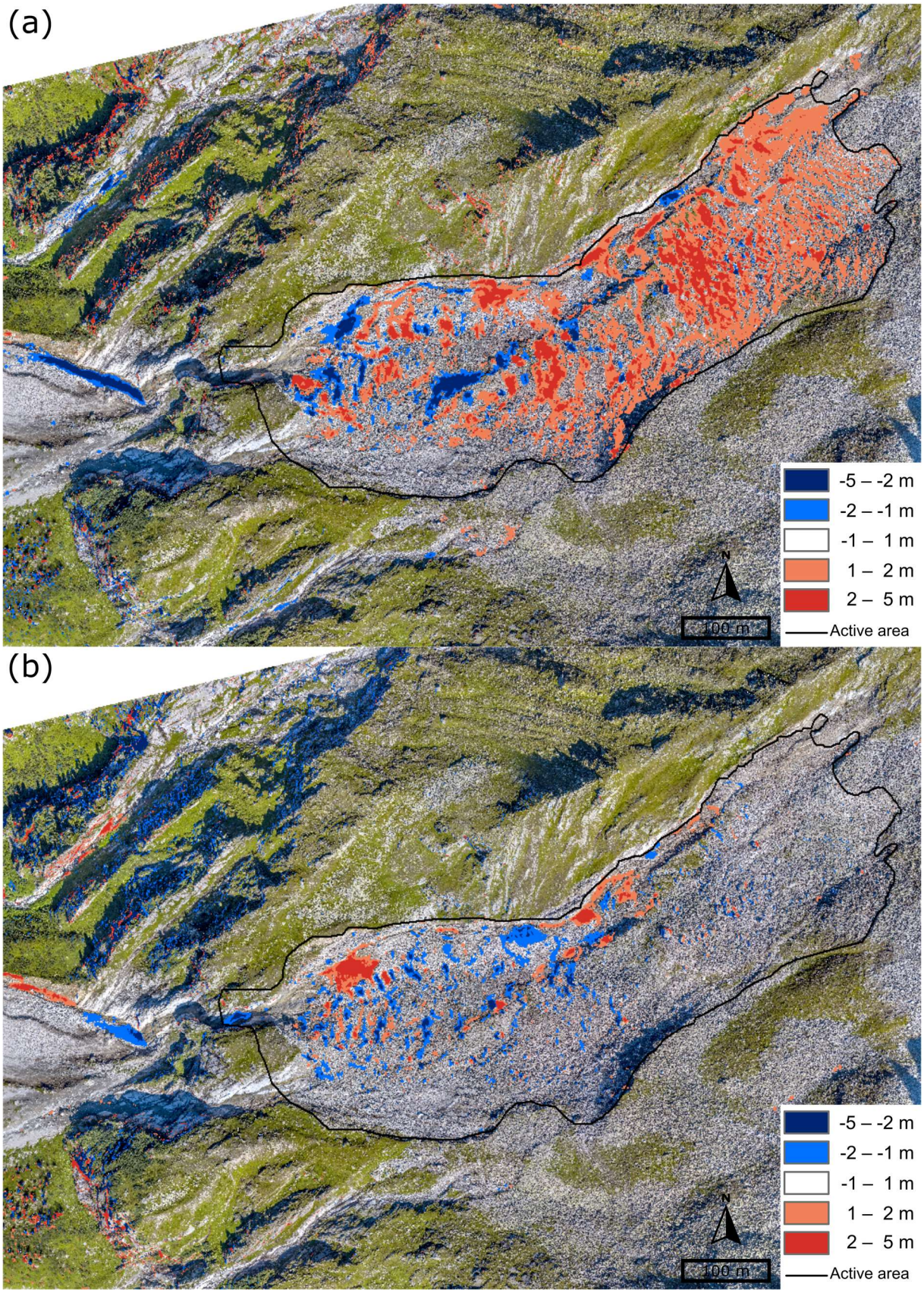

Figure S11 Volume difference calculations of UAS DSM at 0.16 m spatial resolution for Interval I (13.07.2018–24.07.2019, 376 d) and II (24.07.2019–04.09.2019, 42 d). Background UAS orthoimage from 04.09.2019. The solid black line represents the boundary of the active landslide based on field mapping.

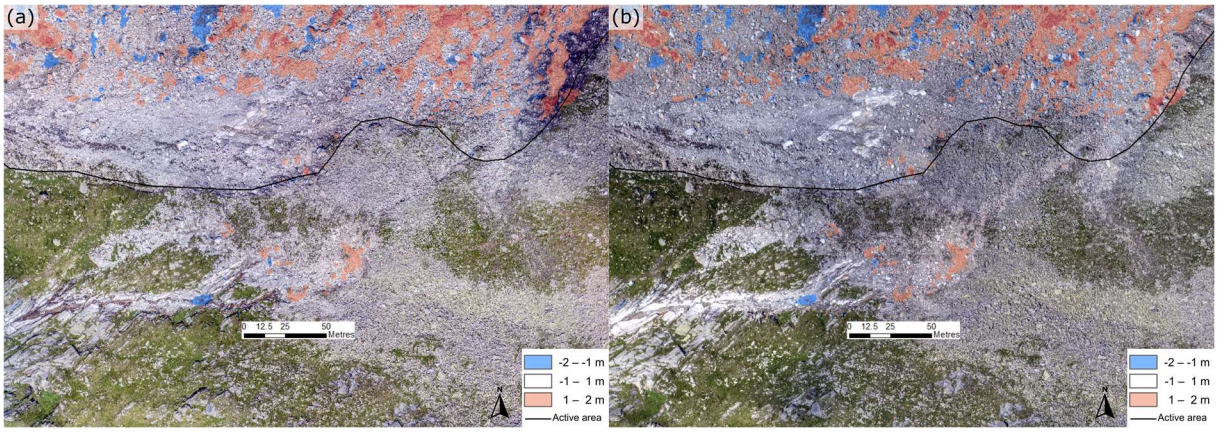

Figure S12 Volume difference calculations for Interval I (13.07.2018–24.07.2019, 376 d) of UAS DSM at 0.16 m spatial resolution with background UAS orthoimages from (a) 13.07.2018 and (b) 24.07.2019. The maps displayed are south of the active area. The solid black line represents the boundary of the active landslide based on field mapping.

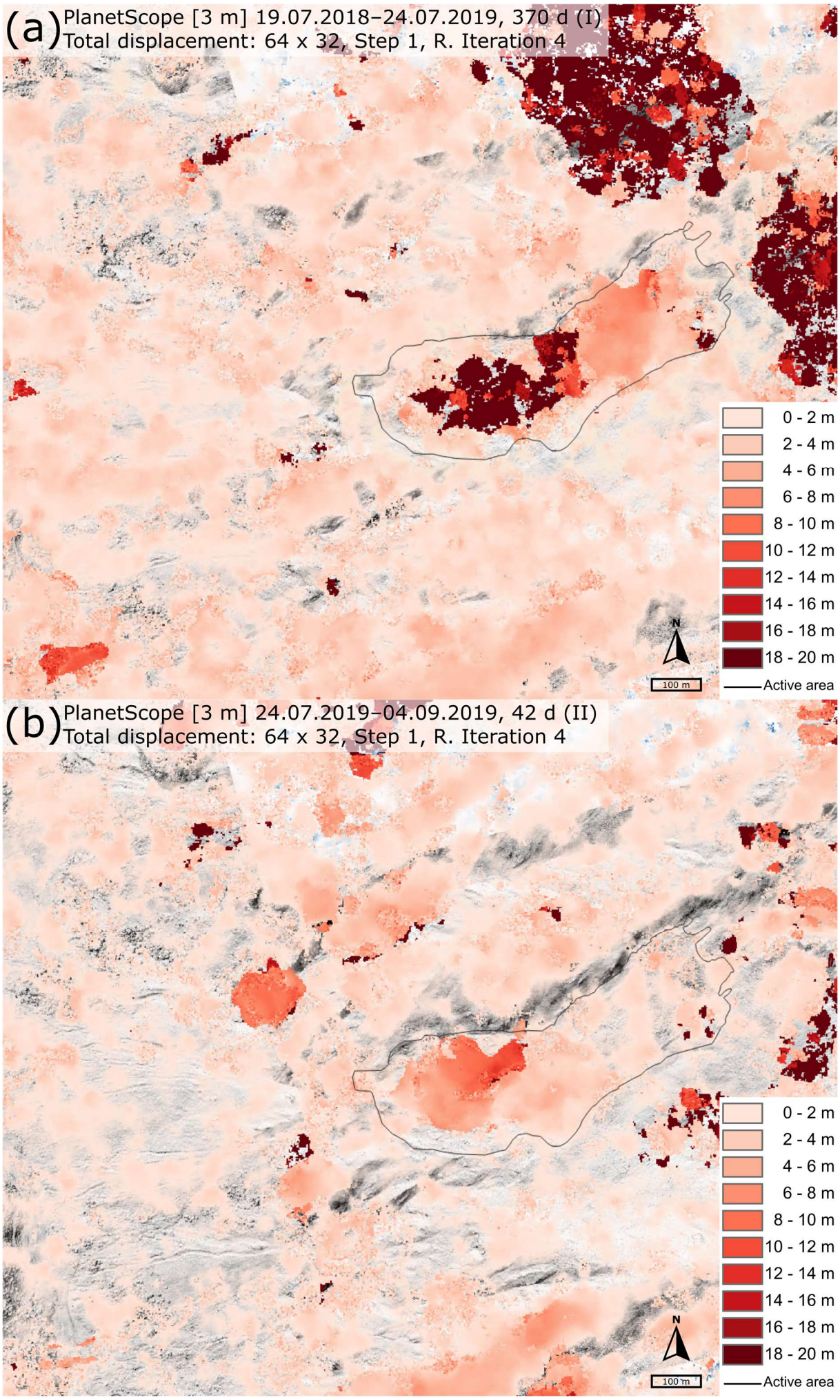
(a)
PlanetScope [3 m] 19.07.2018–24.07.2019, 370 d (I)
Total displacement: 64 x 32, Step 1, R. Iteration 4
0 - 2 m
2 - 4 m
4 - 6 m
6 - 8 m
8 - 10 m
10 - 12 m
12 - 14 m
14 - 16 m
16 - 18 m
18 - 20 m
Active area
N
100 m
(b)
PlanetScope [3 m] 24.07.2019–04.09.2019, 42 d (II)
Total displacement: 64 x 32, Step 1, R. Iteration 4
0 - 2 m
2 - 4 m
4 - 6 m
6 - 8 m
8 - 10 m
10 - 12 m
12 - 14 m
14 - 16 m
16 - 18 m
18 - 20 m
Active area
N
100 m

Figure S13 Results of DIC total displacements of PlanetScope images at 3 m resolution for interval I (a) and interval II (b). The solid black line represents the boundary of the active landslide based on field mapping. Background: hillshade of Lidar DEM, 1 m resolution (© SAGIS).

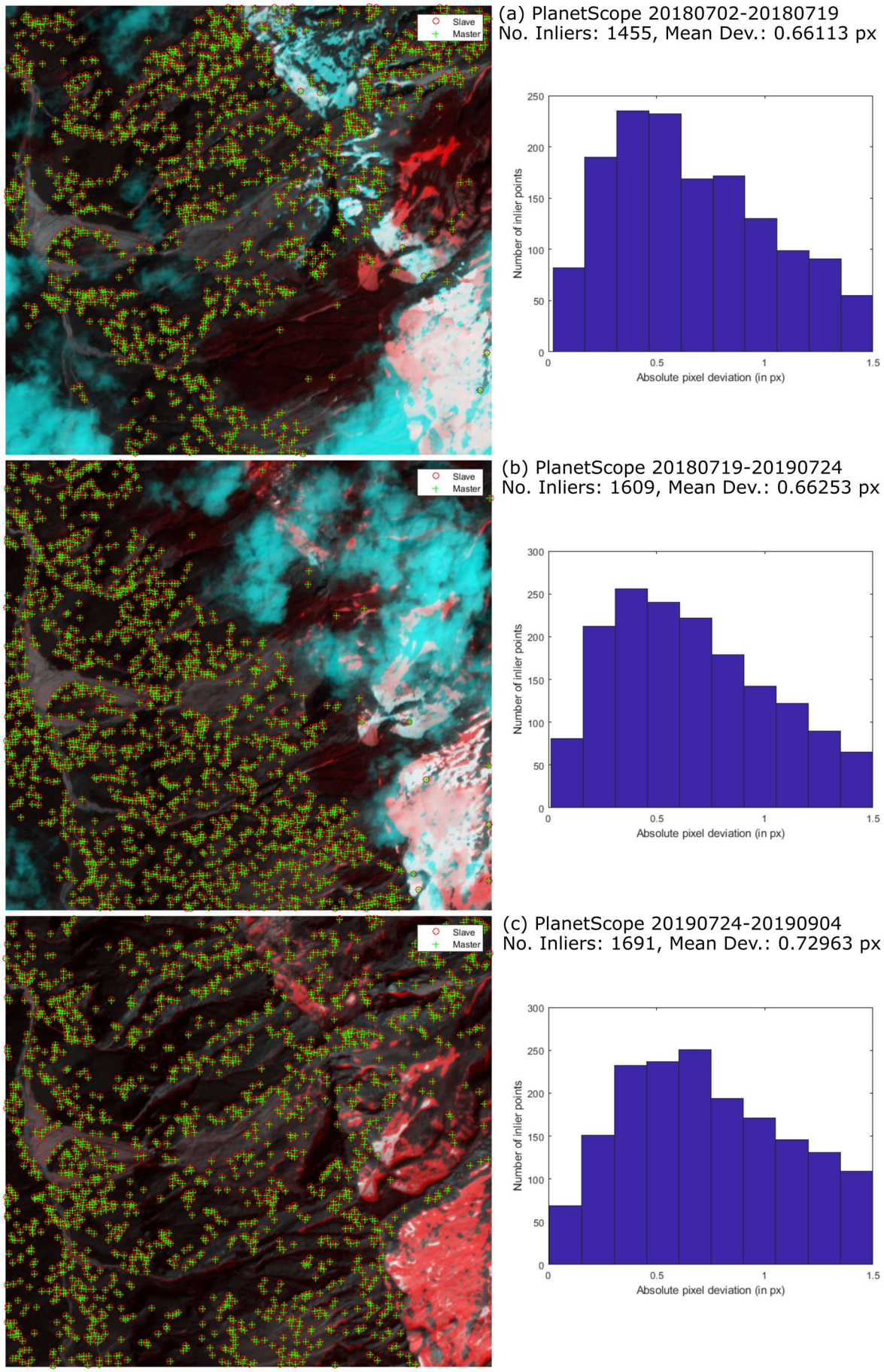

Figure S14 PlanetScope image co-registration for (a) which is discarded in the publication, interval I (b) and interval II (c). Left: distribution of master and slave feature points after transformation. Right: number of transformed inlier feature points of the target image to their corresponding feature matches in the reference image including their distribution and mean distance.

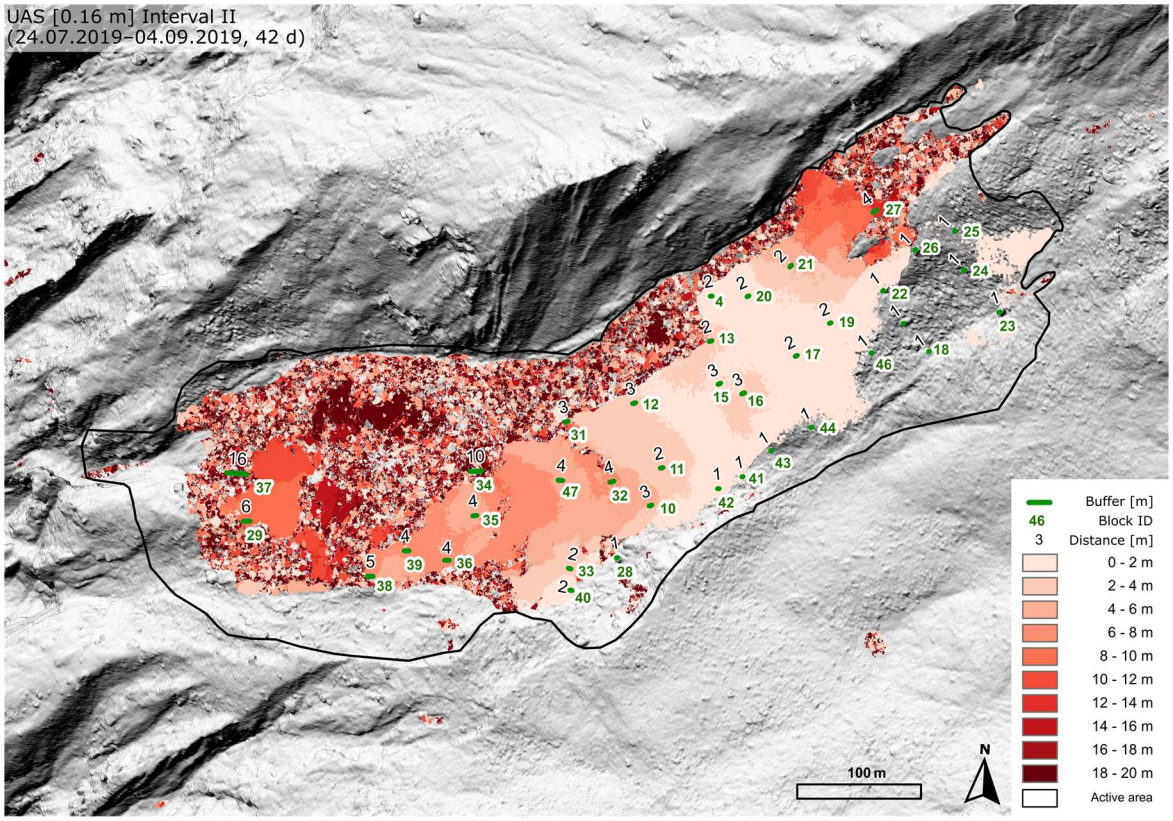

Figure S15 Displacement derived from UAS data at 0.16 m resolution for interval II (24.07.2019–04.09.2019, 42 d) combined with green buffers around boulder trajectories manually measured in the UAS orthophotos in the same time period. Black numbers show boulder travel distance (in metres), block ID in green. The solid black line represents the boundary of the active landslide based on field mapping. Background: UAS hillshade, 24.07.2019 (0.08 m), orientation -3° from north.

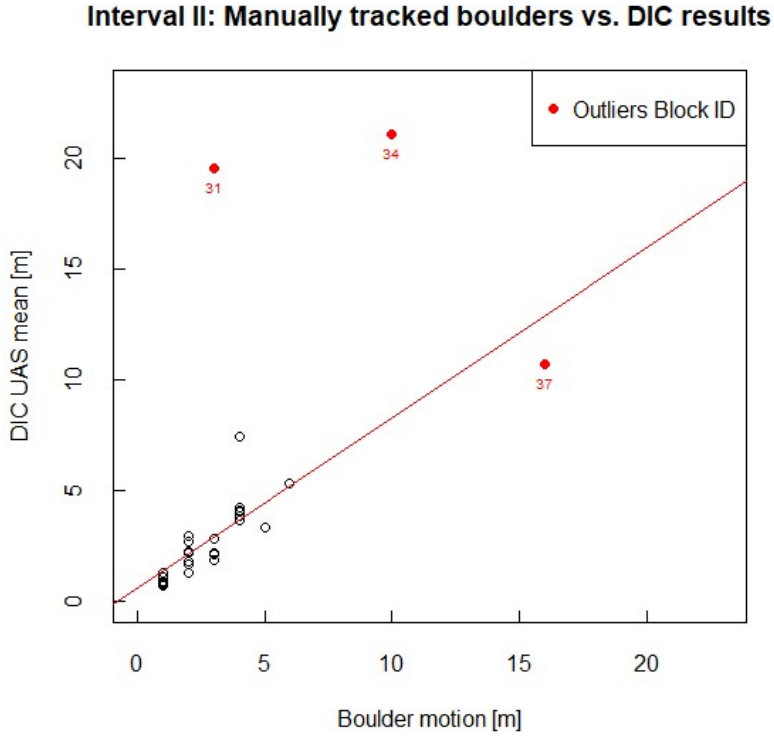

Figure S16 Plot of manually tracked boulder distances (x-axis) compared to the mean of DIC derived total displacement values of buffers around corresponding boulder trajectories (y-axis). Buffers have a 10 cm fringe around the mapped trajectories (see OSM Fig. 15). Corresponding regression line in red excluding the outliers 31, 34 and 37 located within the decorrelated, noisy DIC result and marked as red circles.

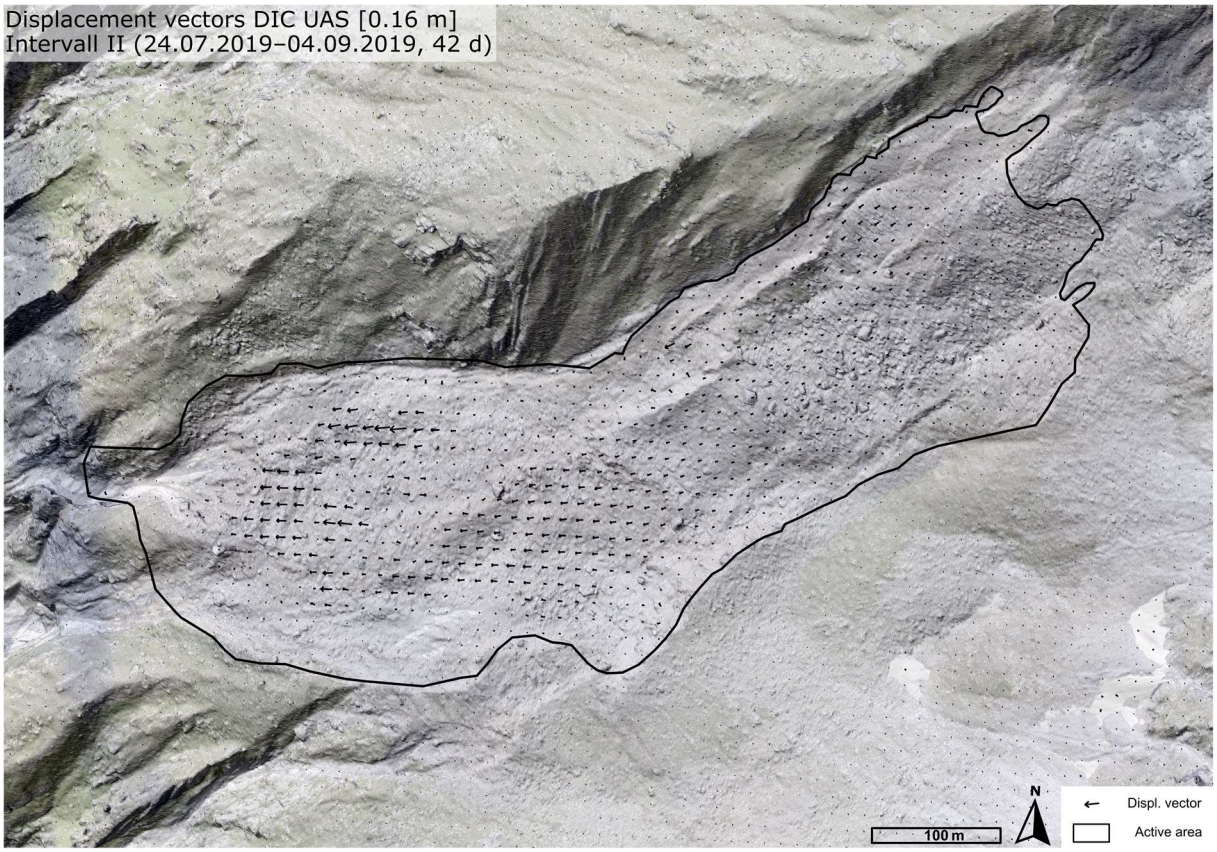

Figure S17 Displacement vectors showing landslide flow (black) derived from COSI-Corr from UAS orthophotos at 0.16 m resolution for interval II (24.07.2019–04.09.2019, 42 d). Background: UAS Orthophoto below a light transparent hillshade.